The Astrophysical Journal, 724:1030–1043, 2010 December 1 doi:10.1088/0004-637X/724/2/1030

THE ACS NEARBY GALAXY SURVEY TREASURY. IX. CONSTRAINING ASYMPTOTIC GIANT BRANCH EVOLUTION WITH OLD METAL-POOR GALAXIES

Léo Girardi[1], Benjamin F. Williams[2], Karoline M. Gilbert[2], Philip Rosenfield[2], Julianne J. Dalcanton[2], Paola Marigo[3], Martha L. Boyer[4], Andrew Dolphin[5], Daniel R. Weisz[6], Jason Melbourne[7], Knut A. G. Olsen[8], Anil C. Seth[9], and Evan Skillman[6]

[1] Osservatorio Astronomico di Padova-INAF, Vicolo dell'Osservatorio 5, I-35122 Padova, Italy
[2] Department of Astronomy, University of Washington, Box 351580, Seattle, WA 98195, USA
[3] Dipartimento di Astronomia, Università di Padova, Vicolo dell'Osservatorio 2, I-35122 Padova, Italy
[4] Space Telescope Science Institute, 3700 San Martin Drive, Baltimore, MD 21218, USA
[5] Raytheon Company, 1151 East Hermans Road, Tucson, AZ 85756, USA
[6] Department of Astronomy, University of Minnesota, 116 Church Street SE, Minneapolis, MN 55455, USA
[7] Caltech Optical Observatories, Division of Physics, Mathematics and Astronomy, Mail Stop 301-17, California Institute of Technology, Pasadena, CA 91125, USA
[8] National Optical Astronomy Observatory, 950 North Cherry Avenue, Tucson, AZ 85719, USA
[9] Harvard-Smithsonian Center for Astrophysics, 60 Garden Street, Cambridge, MA 02138, USA
Received 2010 July 26; accepted 2010 September 23; published 2010 November 10

ABSTRACT

In an attempt to constrain evolutionary models of the asymptotic giant branch (AGB) phase at the limit of low masses and low metallicities, we have examined the luminosity functions and number ratios between AGB and red giant branch (RGB) stars from a sample of resolved galaxies from the ACS Nearby Galaxy Survey Treasury. This database provides *Hubble Space Telescope* optical photometry together with maps of completeness, photometric errors, and star formation histories for dozens of galaxies within 4 Mpc. We select 12 galaxies characterized by predominantly metal-poor populations as indicated by a very steep and blue RGB, and which do not present any indication of recent star formation in their color–magnitude diagrams. Thousands of AGB stars brighter than the tip of the RGB (TRGB) are present in the sample (between 60 and 400 per galaxy), hence, the Poisson noise has little impact in our measurements of the AGB/RGB ratio. We model the photometric data with a few sets of thermally pulsing AGB (TP-AGB) evolutionary models with different prescriptions for the mass loss. This technique allows us to set stringent constraints on the TP-AGB models of low-mass, metal-poor stars (with $M < 1.5\ M_{\odot}$, [Fe/H] $\lesssim -1.0$). Indeed, those which satisfactorily reproduce the observed AGB/RGB ratios have TP-AGB lifetimes between 1.2 and 1.8 Myr, and finish their nuclear burning lives with masses between 0.51 and 0.55 $M_{\odot}$. This is also in good agreement with recent observations of white dwarf masses in the M4 old globular cluster. These constraints can be added to those already derived from Magellanic Cloud star clusters as important mileposts in the arduous process of calibrating AGB evolutionary models.

Key words: stars: general

Online-only material: color figures

1. INTRODUCTION

The thermally pulsing asymptotic giant branch phase (TP-AGB) is both one of the most important and one of the more uncertain phases of stellar evolution. Its importance resides mainly in its sizeable contribution to the integrated light and chemical yields of stellar populations, which are essential for the understanding of galaxy evolution and the interpretation of the light from distant galaxies (e.g., Maraston et al. 2006; Eminian et al. 2008; Conroy et al. 2009; Conroy & Gunn 2010). Its uncertainties derive from a series of circumstances including their complex internal structure; the critical role of difficult-to-model processes such as convective dredge-up, mass-loss, circumstellar dust formation, and long-period variability; and the scarcity of clear-cut and unequivocal observational constraints on their evolution in the most immediate universe.

Gigantic steps are being made in all of these subjects, but the present situation is that the evolutionary timescales of stars in the TP-AGB phase are far from being settled. Uncertainties by a factor of *a few* still exist at the extremes of the age–metallicity region allowed for AGB stars. This contrasts sharply with other evolutionary phases like the main-sequence and red giant branch (RGB), for which the evolutionary times are known with errors smaller than a few tenths, as demonstrated by a large variety of observations (see Gallart et al. 2005 and references therein).

Present-day constraints on the TP-AGB evolution are largely based on observations of stars in the Magellanic Clouds and of the Milky Way (MW). The lifetimes as a function of stellar mass, for slightly subsolar metallicities, can be derived for star counts in Magellanic Cloud clusters (Frogel et al. 1990; van Loon et al. 2005; Girardi & Marigo 2007a). The same can be done for low-mass stars in MW globular clusters. Even for the most populous star clusters, however, AGB stars are few and their counts are affected by large Poisson fluctuations; in the case of MW globular clusters, AGB stars brighter than the tip of the red giant branch (TRGB), and long period variables, practically disappear from observed samples at [Fe/H] $\lesssim -1.0$ (Frogel & Elias 1988; Frogel & Whitelock 1998).

Thus, to obtain useful constraints on the AGB lifetime from star clusters, it is necessary to either sum the star counts in many clusters into age and metallicity bins (e.g., Girardi & Marigo 2007a), or embark on a more detailed study of the dust, chemical, and pulsational properties of individual cluster stars (see, e.g., Lebzelter & Wood 2007; Lebzelter et al. 2008; Kamath et al. 2010 for Magellanic Cloud clusters, and Lebzelter et al. 2006; van Loon et al. 2006; McDonald et al. 2009, 2010; Boyer et al.

2009b, 2010 for MW globular clusters). Less direct constraints on AGB evolution come from integrated cluster properties, such as their colors and surface brightness fluctuations (see, e.g., Maraston 2005; Pessev et al. 2008; Raimondo 2009; Conroy et al. 2009; Conroy & Gunn 2010), which by their very nature cannot disentangle different evolutionary properties such as stellar luminosities, lifetimes, and chemical types, and hence often provide somewhat ambiguous constraints on the numbers of stars at different evolutionary stages. It may happen, for instance, that TP-AGB models which do not consider the third dredge-up and the formation of carbon stars (such as the BaSTI ones; Cordier et al. 2007), or models in which carbon stars are shifted to the high effective temperature ($T_{\rm eff}$) range of 4000–3100 K (Conroy et al. 2009; Conroy & Gunn 2010, with their $\log T_{\rm eff}$ shift of $\sim$+0.1 dex for TP-AGB stars at Magellanic Cloud metallicities), provide acceptable (but spurious) fits to integrated colors of Magellanic Cloud clusters. Unfortunately, the properties of these models are inconsistent with the most basic observations of over 10,000 C-type AGB stars in the Magellanic Clouds (see Nikolaev & Weinberg 2000; Cioni & Habing 2003) with a significant fraction being at $3100 > T_{\rm eff}({\rm K}) > 2650$ (Groenewegen et al. 2009). Such high discrepancies and gaps in the models remain hidden when only the integrated properties are examined.

The problem of low number counts in star clusters could, in principle, be circumvented by using AGB star counts in entire galaxies, but, in practice, this implies meeting a series of difficulties. For galaxies with moderate-to-high metallicities, the AGB develops at low effective temperatures, and consequently near-infrared photometry is required to unveil them, as dramatically demonstrated by the Magellanic Clouds (Frogel et al. 1990; Cioni et al. 2000; Weinberg & Nikolaev 2001). Moreover, since a non-negligible fraction of the AGB population becomes dust-enshrouded, mid-infrared data are necessary for a complete census of the AGB population (e.g., Blum et al. 2006; Bolatto et al. 2007; Boyer et al. 2009a).

At the limit of very low metallicities, the nearest low surface brightness dwarf spheroidal galaxies (dSph) seem to be particularly useful for the study of their AGB populations because they appear uncrowded at magnitudes accessible with present-day 4 m class telescopes equipped with near-infrared cameras. Indeed, Gullieuszik et al. (2008) and Held et al. (2010) are able to derive important indications from ground-based data of the Leo II and Leo I dSphs (see also Lagadec et al. 2008 for Fornax and Sagittarius). The main uncertainties in these works derive from the small numbers of AGB stars, from the high MW foreground contamination, and the uncertainties in the dSphs star formation histories (SFHs). Also, Boyer et al. (2009a) call attention to the large fraction (30%–40%) of AGB stars in dwarf irregulars (dIrr) which are bright in mid-infrared light, but are either missing or misclassified in optical studies because they are enshrouded in thick dust shells. It is still not clear whether this fraction is also representative of dSphs.

The possibilities for a better calibration of AGB luminosities and lifetimes become much wider when milliarcsecond resolution imaging is available. A good example is provided by Melbourne et al. (2010), who use images taken with the Advanced Camera for Surveys (*HST*/ACS) in the *I* band ($F814W$) together with Keck Adaptive Optics (AO) in *K* to study the AGB population of the dIrr KKH 98 at a distance of 2.5 Mpc. This work clearly demonstrates the utility of moving toward more distant resolved dwarf galaxies, for which (1) more stars can be observed in a single pointing, even considering the small field of view available for ACS and AO, and (2) the MW foreground becomes dramatically smaller. On the other hand, some potential disadvantages of these targets are also evident: (1) they present SFHs that are somewhat more uncertain than the nearest dSphs; (2) there is no spectroscopic information to allow a clear-cut separation between the hottest C- and O-rich stars (cooler stars, instead, are well separated by their infrared colors), which limits the analysis of aspects related to the third dredge-up events in the AGB; (3) the mid-infrared photometry is also not available, due to the limited resolution of *Spitzer* and AKARI, hence limiting the analysis to non-obscured AGB stars; and (4) the chance of crowding/blending of AGB and RGB stars also increases with distance.

A result common to the low-metallicity dwarf galaxies studied by Gullieuszik et al. (2008), Held et al. (2010), and Melbourne et al. (2010) is that the TP-AGB lifetimes from Marigo & Girardi (2007, hereafter MG07) and Marigo et al. (2008) models are, apparently, largely overestimated. The reason for this is still not clear, but is possibly due to the underestimation of the mass-loss rates at low metallicities. As a concurring factor, the circumstellar extinction presently assumed in the models may be somewhat underestimated, as suggested by the *Spitzer* observations of nearby dwarf irregulars by Jackson et al. (2007a, 2007b) and Boyer et al. (2009a). Regardless, it is likely that the problem is limited to low metallicities, since the MG07 TP-AGB models have been calibrated in the intermediate-metallicity Magellanic Clouds. Their evolutionary behavior at very low metallicities can be considered as either educated guesses, or extrapolations of the behavior met at intermediate metallicities, since they are a result of the straight application of theoretically uncertain metallicity dependences.

In this paper, we use *Hubble Space Telescope* (*HST*) optical data from the ACS Nearby Galaxy Survey Treasury (ANGST) survey to derive constraints on the AGB evolution for a set of metal-poor galaxies in which the recent star formation activity is generally very low, if not absent. Our target is to derive constraints on the optically visible TP-AGB lifetimes of low-mass, metal-poor stars. The advantage of using a set of Mpc-distant galaxies is clear: we will have thousands of AGB stars in our samples, reducing Poisson noise to a minimum. The price to pay, as in the case of Melbourne et al. (2010), is that our analysis can be affected by uncertainties in the SFHs of individual galaxies. The hope however is that these SFH errors become less relevant when averaged over a large sample of galaxies.

In Section 2, we describe the data used in this work. In Section 3, we model the data using two different sets of TP-AGB models, deriving clear quantitative constraints on them. We then provide a revised set of TP-AGB tracks that brings models and observations into better agreement.

2. THE DATA

2.1. The ANGST/ANGRRR Photometry Database

We used data from the ANGST[10] (Dalcanton et al. 2009) and from the "Archive of Nearby Galaxies: Reduce, Reuse, Recycle" (ANGRRR)[11] databases. These two programs have archived stellar photometry for tens of millions of stars in nearby galaxies outside the Local Group, based on images taken with the ACS and the Wide Field Planetary Camera

[10] http://www.nearbygalaxies.org, http://archive.stsci.edu/prepds/angst/
[11] http://archive.stsci.edu/prepds/angrrr

2 (WFPC2) on the *HST*. The imaging primarily used blue observations in the $F475W$, $F555W$, or $F606W$ filters, and $F814W$ for the red filter. The photometry was performed using DOLPHOT[12] and HSTPHOT[13] (for ACS and WFPC2 imaging, respectively; Dolphin 2000), as described fully in Dalcanton et al. (2009) and Williams et al. (2009). The depth of the resulting color–magnitude diagrams (CMDs) varies with distance, crowding, and exposure time, but reaches several magnitudes below the TRGB in all cases, and below the red clump ($M_I \sim -0.5$ mag) in all but two of the cases we analyze here.

For this paper, the photometry from the first data release for ANGST and ANGRRR has been supplemented with extensive artificial star tests. For each of the fields studied, a minimum of 100,000 artificial star experiments were performed to determine the completeness and errors as a function of color and magnitude. In each test, one star of known color and magnitude was added to the data, and the photometry routine was re-executed to determine the difference between the input and output magnitudes if the star was recovered.

SFHs were determined by fitting the observed CMDs with the MATCH fitting package (Dolphin 2002). The parameters of MATCH were set to match those used by Williams et al. (2009). In brief, a Salpeter (1955) IMF was used to generate a base set of Hess diagrams using the isochrones of Girardi et al. (2002; with updates in Marigo et al. 2008) and the error and completeness from our artificial star tests. The best-fit combination of this base set of diagrams was then determined using the statistics described in Dolphin (2002). First, the fit was performed on the full data set brightward of the 50% completeness limit as determined by our artificial star tests. Then, the fit was repeated excluding all data brightward of the TRGB. This second fit allowed us to quantify the effects of the bright AGB stars on the resulting SFH (as discussed in Section 3.2).

We further analyzed the CMDs to estimate extinctions A_V, distance moduli $(m-M)_0$, and the magnitude of the TRGB. The total extinction and distance moduli are determined automatically by MATCH, based on the optimal reddening and distance needed to reproduce the observed CMD (see the full discussion in Williams et al. 2009), assuming $R_V = 3.1$ at optical wavelengths. Uncertainties are determined by identifying the range over which A_V and $(m-M)_0$ can vary without producing a statistically significant reduction in the quality of the fit to the observed CMD.

2.2. The Galaxy Sample and Their SFHs

We chose galaxies for our sample based on two primary criteria—metallicity and mean stellar age. The first restriction results from our desire to analyze only the galaxies in which the ANGST/ANGRRR optical data contain a nearly complete census of the AGB population. This requirement naturally limits our work to galaxies with metal-poor populations (say [Fe/H] $\lesssim -1.2$). At these metallicities, the upper AGB develops at $T_{\rm eff} > 4000$ K and colors $F475W-F814W < 2.4$, or $F606W-F814W < 1.2$, and still falls at the plateau of the BC–$T_{\rm eff}$ relations (Figure 1). Bolometric corrections for low-metallicity AGB stars are thus close to their minimum values, ensuring that the brighter stars really do appear at the smaller magnitudes. In contrast, for redder, high-metallicity AGB stars, bolometric corrections become significant and increase steadily with color. Redder AGB stars thus become progressively less accessible in the optical, and instead require near-infrared photometry to extend the complete AGB counts toward the region of lower $T_{\rm eff}$, which corresponds to more metal-rich galaxies.

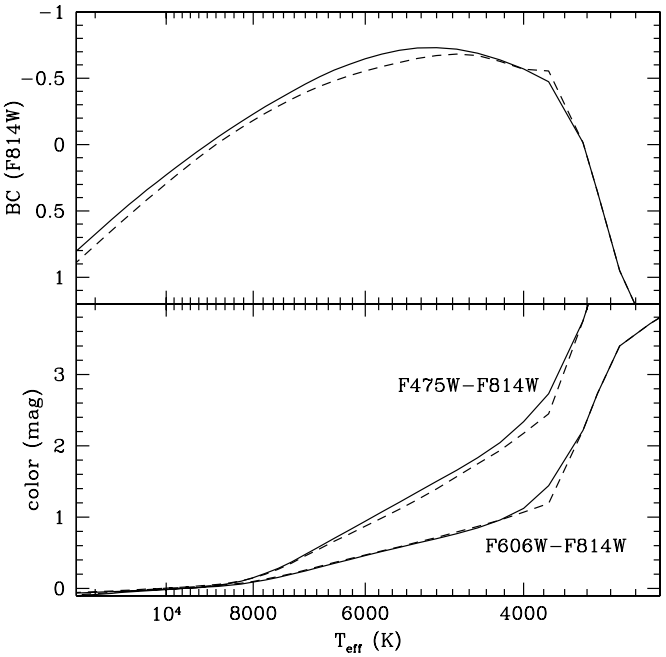

Figure 1. Top panel: $F814W$-band bolometric corrections as a function of $T_{\rm eff}$, for both [Fe/H] = 0 (continuous line) and [Fe/H] = −2 (dashed line). Bottom panel: the $T_{\rm eff}$–color relations for both $F475W-F814W$ and $F606W-F814W$, for the same metallicities. These relations are described in Girardi et al. (2008). The small kinks at $T_{\rm eff} \sim 3800$ K correspond to the transition between Castelli & Kurucz (2003, for $\log g = 2$) and Fluks et al. (1994) model atmospheres.

We further restrict the galaxy sample to regions that have a simple-to-interpret SFH, with AGB stars limited to a well-defined region of the age–metallicity plane. This request limits us to galaxies dominated by old stars, for which there is no sign of recent or intermediate-age star formation. Thanks to the steep mass–main-sequence lifetime relation, the absence of populations younger than 3 Gyr ensures that the evolved stars have initial masses confined to a narrow interval, of roughly 0.8–1.4 $M_\odot$. The AGB star counts in these galaxies should then provide clear constraints on the evolution of low-mass stars.

Based on these two conditions, we have selected a sample of galaxies for which a visual inspection of the CMD revealed: (1) an almost vertical RGB, with the TRGB at $F475W-F814W \lesssim 2$, or $F606W-F814W \lesssim 1$ so as to indicate low metallicity and $\mathrm{BC}_{F814W} \lesssim 0.5$ (Figure 1), and low foreground extinction, and (2) no evidence for recent and intermediate-age star formation, as indicated by an absence of any younger main sequence and helium burning sequence above the red clump/HB. This latter restriction eliminates galaxies with star formation in the most recent 0.5 Gyr, but may admit galaxies with some amount of star formation at intermediate ages. A full analysis of the SFHs can be found in D. R. Weisz et al. (2011, in preparation).

Although our selection considered both ACS and WFPC2 data, it turns out that the final sample contains ACS data only.

The left panels in Figure 2 illustrate the CMDs for all the selected galaxies and galaxy regions. Their basic properties and parameters are listed in Table 1.

[12] http://purcell.as.arizona.edu/dolphot
[13] http://purcell.as.arizona.edu/hstphot

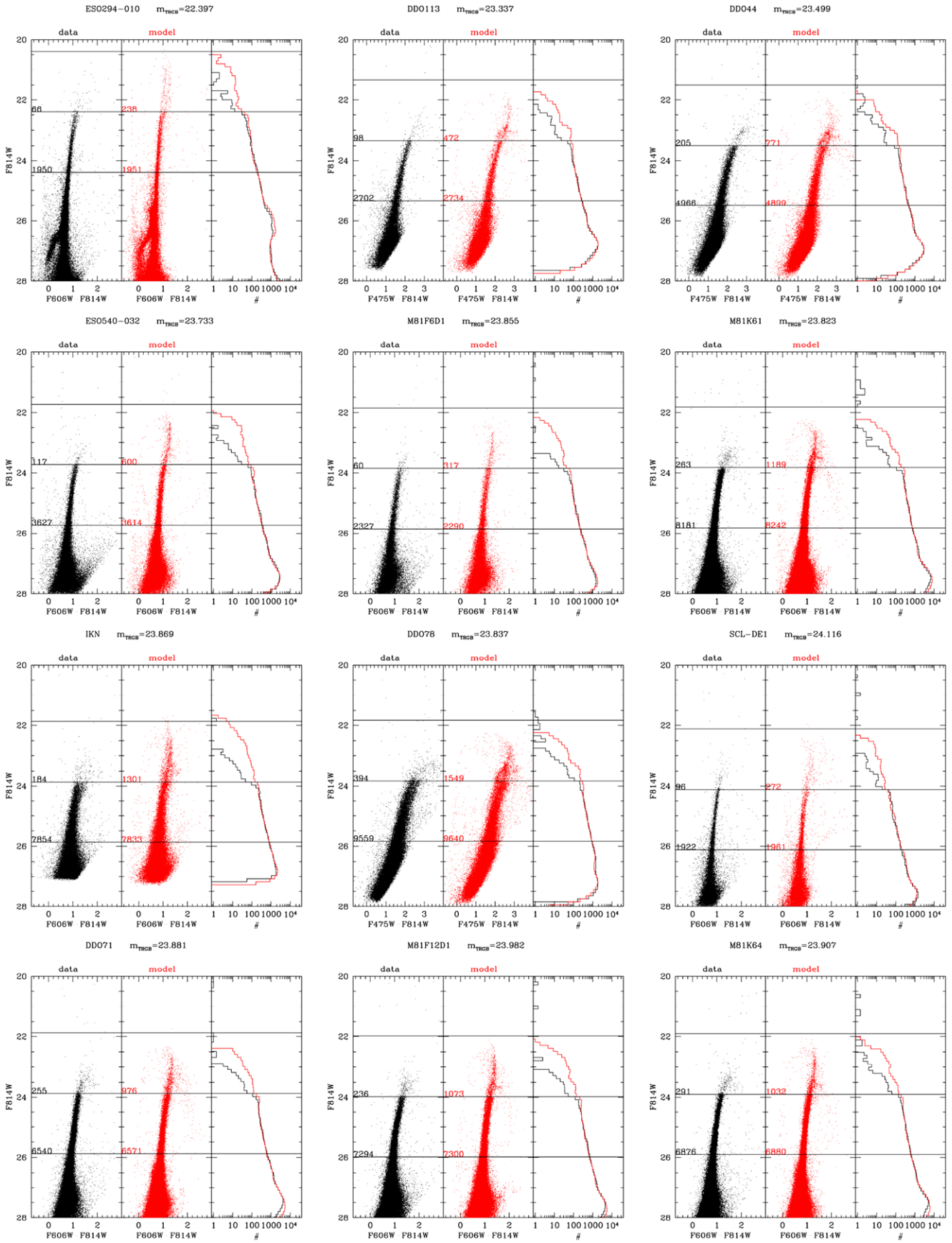

Figure 2. Data and models used in this work, for all galaxies and galaxy regions in our sample. Left panels: the observed CMD from ANGST/ANGRRR. The horizontal lines mark the TRGB and upper and lower magnitude limits of the stars considered to be in the upper RGB and AGB. Their total numbers are marked inside the boxes. Middle panels: the same as in the left panel, but for the model CMD from TRILEGAL, with the default set of TP-AGB models (Marigo et al. 2008) and scaled to present the same number of upper RGB stars. Right panels: a comparison between the observed (black) and model (red or gray) luminosity functions.

(A color version of this figure is available in the online journal.)

Table 1
Basic Parameters of Our Galaxy Sample

Target/Name	Filters	A_V	$m_{\rm TRGB}$	$m_{50\%\rm complete}$	$(m-M)_0$	$N_{\rm RGB}$	$N_{\rm AGB}$	$\frac{N_{\rm AGB}}{N_{\rm RGB}}$
ESO294-010	$F606W$, $F814W$	0.018	22.397 ± 0.008	28.25	26.434	1950	66	0.034 ± 0.004
DDO113	$F475W$, $F814W$	0.063	23.337 ± 0.026	27.43	27.349	2702	98	0.036 ± 0.004
DDO44	$F475W$, $F814W$	0.129	23.499 ± 0.015	27.61	27.454	4966	205	0.041 ± 0.003
ESO540-032	$F606W$, $F814W$	0.064	23.733 ± 0.020	27.83	27.743	3627	117	0.032 ± 0.003
M81F6D1	$F606W$, $F814W$	0.241	23.855 ± 0.010	27.85	27.737	2326	60	0.026 ± 0.003
M81K61	$F606W$, $F814W$	0.226	23.823 ± 0.042	28.05	27.716	8181	263	0.032 ± 0.002
IKN	$F606W$, $F814W$	0.181	23.869 ± 0.019	26.97	27.786	7854	184	0.023 ± 0.002
DDO78	$F475W$, $F814W$	0.066	23.837 ± 0.017	27.55	27.818	9559	394	0.041 ± 0.002
SCL-DE1	$F606W$, $F814W$	0.046	24.116 ± 0.023	28.41	28.110	1922	96	0.050 ± 0.005
DDO71	$F606W$, $F814W$	0.303	23.881 ± 0.019	28.05	27.740	6540	255	0.039 ± 0.002
M81F12D1	$F606W$, $F814W$	0.442	23.982 ± 0.013	28.03	27.749	7294	236	0.032 ± 0.002
M81K64	$F606W$, $F814W$	0.165	23.907 ± 0.009	28.42	27.852	6876	291	0.042 ± 0.003
Total						65771	2265	0.0344 ± 0.0007

Note. A_V and $(m-M)_0$ come from the best MATCH solution.

2.3. Selecting AGB and RGB Stars

To identify the location of RGB stars, we adopted the magnitude of the TRGB ($m_{\rm TRGB}$) from Dalcanton et al. (2009), who identified the TRGB in uncrowded low extinction regions of each galaxy using the edge-detection method of Méndez et al. (2002). The TRGB magnitude can also be converted into a distance modulus, using the foreground extinction derived by Schlegel et al. (1998), and the absolute magnitude of the TRGB in the isochrones of Marigo et al. (2008) at the observed color of the RGB stars used to derive the TRGB. The TRGB-based distance modulus does not necessarily agree with the one reported by MATCH, since the latter can be biased toward larger distances in an attempt to better fit the magnitude of the well-populated red clump, which is known to be faint in the Marigo et al. (2008) isochrones currently used in MATCH. In what follows, we use the $(m-M)_0$ and A_V derived from MATCH for generating artificial CMDs. However, for isolating AGB stars, we use the empirically determined value of $m_{\rm TRGB}$, as given in Table 1.

An interval of two magnitudes above the TRGB defines the "AGB sample." In all cases, it includes the bulk of (if not all) stars brighter than the TRGB. Their number, $N_{\rm AGB}$, is typically between 60 and 400 per galaxy.

The RGB sample, instead, is defined over 2 mag below the TRGB. This sample has, typically, a completeness above 95%, and about 30 times more stars than in the AGB sample.

The number ratios between AGB and RGB stars, $N_{\rm AGB}/N_{\rm RGB}$, are presented in Table 1, together with the 1σ random errors.

The AGB sample as above defined is contaminated by a few RGB stars at its faintest magnitude bins because of the scattering of stars to brighter magnitudes by photometric errors and binaries. For the galaxies with the smallest $N_{\rm AGB}/N_{\rm RGB}$, the effect is such that this ratio can be increased by up to 20% with respect to its true value. As we will see below, this is a marginal effect considering the large discrepancies—of a few times—between present models and the observations. Moreover, the scattering of RGB stars to brighter magnitudes is fully taken into account in our simulations (Section 3), so that no inconsistency results from counting a few RGB stars in the AGB sample. On the other hand, the RGB sample contains both the initial sub-luminous section of the TP-AGB phase and the excursions to low-luminosities driven by thermal pulses, as well as stars leaving the early-AGB phase. Based on evolutionary models, we estimate that this contamination, in the worst cases, is just a few percent. Moreover, the numbers of early-AGB stars are expected to be quite insensitive to the uncertainties in the mass-loss prescriptions, which instead plague the TP-AGB stars above the TRGB.

2.4. Uncertainties in the SFH and AGB/RGB Ratio

The measured $N_{\rm AGB}/N_{\rm RGB}$ ratios have values comprised between 0.023 and 0.050. Random errors are, in all cases, smaller than 20%. The mean value derived by adding all stars in the sample is 0.0344 ± 0.0007. Clearly, the random noise in the relative number of AGB stars is less of a concern in our data set. The main point of concern instead is in the correctness of the SFHs for the host galaxies, which is crucial for the interpretation of the $N_{\rm AGB}/N_{\rm RGB}$ ratios.

As we show below, the current isochrones overpopulate the AGB sequences, potentially biasing our SFHs to low star formation rates and intermediate ages when these stars are included in the fit of the CMD. We therefore re-derive the SFHs excluding AGB stars, taking care to keep all other aspects of the fitting identical. Specifically, we exclude CMD regions above the TRGB, and those with either $F606W-F814W > 3.5$ or $F475W-F814W > 4.5$ (depending on the filters used in the observations) from our fitting. The resulting SFHs correspond to the "no-AGB" cases in Table 2. They differ little from the default "with-AGB" cases, indicating that the structure of the red clump has far more influence on the inferred SFH at intermediate ages with the weighting scheme currently employed by MATCH.

We also have applied the "Z-inc" option to derive SFH. It consists of limiting the number of free parameters in our fits by forcing the fit to only attempt solutions where the metallicity remains constant or increases with time. The history returning the best fit to the CMD is then selected. This process is important in some cases where the photometry depth or the number of stars is insufficient to reliably separate the effects of age from those of metallicity.

The initial columns in Table 2 summarize the results in terms of SFH, presenting the fraction of the SFH in the age intervals from 0 to 1 Gyr, and from 1 to 3 Gyr, for all cases of SFH recovery that were tested. It turns out, as expected, that all galaxies but SCL-DE1 present a very small amount of their SFH at ages <1 Gyr, and roughly 10% at 1–3 Gyr. The SFHs for the different cases (with and without AGB stars, default or Z-inc) do agree well considering the typical error bars in this

Table 2
The SFR and AGB/RGB Ratios

Target/Name	Which SFH					N_{AGB}/N_{RGB}			
	AGB?	Z-inc?	$\frac{SFR_{<1\,Gyr}}{SFR_{tot}}$	$\frac{SFR_{1-3\,Gyr}}{SFR_{tot}}$	⟨[Fe/H]⟩	Observed	Ma08	Case A	Case B
ESO294-010	Y	N	0.01	0.07	−1.68	0.034 ± 0.004	0.149	0.020	0.020
	Y	Y	0.01	0.07	−1.63		0.131	0.021	0.019
	N	N	0.02	0.08	−1.75		0.133	0.025	0.019
	N	Y	0.02	0.09	−1.74		0.155	0.021	0.022
DDO113	Y	N	0.02	0.23	−1.55	0.036 ± 0.004	0.147	0.068	0.073
	Y	Y	0.01	0.17	−1.57		0.144	0.070	0.062
	N	N	0.03	0.16	−1.44		0.162	0.076	0.068
	N	Y	0.03	0.17	−1.42		0.155	0.066	0.075
DDO44	Y	N	0.01	0.21	−1.20	0.041 ± 0.003	0.147	0.070	0.069
	Y	Y	0.01	0.19	−1.13		0.131	0.039	0.050
	N	N	0.02	0.11	−1.13		0.150	0.064	0.067
	N	Y	0.02	0.21	−1.14		0.146	0.065	0.066
ESO540-032	Y	N	0.03	0.05	−1.42	0.032 ± 0.003	0.146	0.055	0.049
	Y	Y	0.02	0.03	−1.47		0.166	0.058	0.045
	N	N	0.03	0.07	−1.56		0.162	0.043	0.042
	N	Y	0.02	0.03	−1.48		0.162	0.044	0.046
M81F6D1	Y	N	0.01	0.04	−1.12	0.026 ± 0.003	0.133	0.024	0.026
	Y	Y	0.01	0.02	−1.25		0.145	0.033	0.030
	N	N	0.02	0.06	−1.17		0.137	0.030	0.028
	N	Y	0.02	0.01	−1.20		0.149	0.025	0.026
M81K61	Y	N	0.01	0.04	−1.12	0.032 ± 0.002	0.112	0.020	0.021
	Y	Y	0.01	0.02	−1.25		0.122	0.034	0.035
	N	N	0.02	0.06	−1.17		0.135	0.039	0.043
	N	Y	0.02	0.01	−1.20		0.147	0.044	0.047
IKN	Y	N	0.02	0.03	−1.11	0.023 ± 0.002	0.116	0.029	0.031
	Y	Y	0.02	0.05	−1.49		0.124	0.028	0.031
	N	N	0.03	0.00	−1.17		0.160	0.046	0.040
	N	Y	0.04	0.00	−1.55		0.158	0.033	0.033
DDO78	Y	N	0.01	0.14	−1.12	0.041 ± 0.002	0.127	0.069	0.071
	Y	Y	0.01	0.11	−1.10		0.156	0.089	0.088
	N	N	0.01	0.16	−1.17		0.150	0.081	0.079
	N	Y	0.01	0.15	−1.09		0.164	0.095	0.102
SCL-DE1	Y	N	0.10	0.27	−0.79	0.050 ± 0.005	0.314	0.269	0.251
	Y	Y	0.06	0.11	−1.57		0.358	0.274	0.275
	N	N	0.06	0.38	−0.98		0.136	0.061	0.052
	N	Y	0.08	0.05	−1.63		0.212	0.105	0.099
DDO71	Y	N	0.01	0.12	−1.05	0.039 ± 0.002	0.121	0.021	0.023
	Y	Y	0.02	0.08	−1.19		0.115	0.029	0.030
	N	N	0.02	0.11	−1.06		0.141	0.040	0.046
	N	Y	0.01	0.07	−1.17		0.135	0.038	0.043
M81F12D1	Y	N	0.01	0.08	−1.17	0.032 ± 0.002	0.127	0.020	0.018
	Y	Y	0.01	0.03	−1.29		0.125	0.023	0.024
	N	N	0.01	0.05	−1.15		0.142	0.034	0.032
	N	Y	0.01	0.02	−1.19		0.130	0.023	0.024
M81K64	Y	N	0.01	0.08	−1.25	0.042 ± 0.003	0.134	0.022	0.023
	Y	Y	0.01	0.08	−1.32		0.138	0.030	0.025
	N	N	0.01	0.07	−1.26		0.143	0.038	0.033
	N	Y	0.01	0.06	−1.30		0.146	0.035	0.039
Results for mid-to-lowest density rings of galaxies									
ESO540-032	N	N	0.03	0.06	−1.49	0.028 ± 0.004	0.162	0.059	0.058
DDO113	N	N	0.02	0.13	−1.45	0.037 ± 0.005	0.153	0.071	0.052
M81K61	N	N	0.01	0.11	−1.21	0.029 ± 0.003	0.143	0.043	0.042
DDO78	N	N	0.02	0.12	−1.24	0.038 ± 0.003	0.169	0.070	0.076

kind of measurement, again with the exception of SCL-DE1 for which the Z-inc cases provide significantly older SFHs.

3. MODELING THE DATA: METHOD AND RESULTS

3.1. Code and Method

To model the ANGST/ANGRRR data, we use a recent version of the TRILEGAL code (Girardi et al. 2005), which generates multi-band mock catalogs of resolved stellar populations for a given distribution of distances and extinctions, following some specified SFH and age–metallicity relation. The original code has been expanded in several aspects to deal with the complex features of TP-AGB stars (Girardi & Marigo 2007b, and later work), including different bolometric corrections and T_{eff}–color relations for O-rich and C-rich stars, luminosity (L) and T_{eff} variations driven by thermal pulses, and obscuration by

circumstellar dust. In order to take these effects onto account, the code keeps track of a series of stellar parameters, such as the surface chemical composition, mass loss, and the period and mode of the long-period variability. The dust composition has been assumed to be 60% silicate plus 40% AlOx for O-rich stars, and 85% amorphous carbon plus 15% SiC for C-rich stars from Groenewegen (2006).

The stellar evolutionary tracks are the same ones contained in the Marigo et al. (2008) isochrones and used by MATCH to derive the SFH of our galaxy sample. The transformations from L and $T_{\rm eff}$ to the *HST* photometry are described in Girardi et al. (2008); however, we have updated it to use the latest transformations for C-type stars from Aringer et al. (2009), and the total ACS/WFC throughput curves and zero points appropriate for post-July 2006 observations (Mack et al. 2007; Bohlin 2007).[14]

Alternative sets of TP-AGB tracks have been specifically calculated for this work, as described below in Section 3.4. TRILEGAL allows these tracks to be replaced quickly and with minimal human effort.

We first start modeling the data for the complete sample of galaxies in Table 1, using the same stellar models which were already used to derive the SFH, but using TRILEGAL instead of MATCH. TRILEGAL simulates the photometry starting from the SFH file and shifts the data to the right distance modulus and extinction. The simulations include stars up to 2 mag fainter than the faintest observed one.

In order to properly account for the real completeness and photometric errors in our simulations, we proceed as follows. For each simulated star, an artificial star of similar color and magnitude is randomly extracted from the existing catalog of artificial stars from HSTPHOT/DOLPHOT. If that artificial star has been detected by the photometry software, the differences between the input colors and magnitudes and the output ones are applied to the simulated star; otherwise, the same object is thrown away.

3.2. Results Using MG07 TP-AGB Tracks

Results from this exercise are shown in Figure 2. Note that the simulations are forced to have a number of bright RGB stars (within 2 mag of the TRGB) consistent with the observed one within 1σ. One can note that these simulations resemble very much the observations, except for the TP-AGB regime, for which there is a clear excess of simulated stars, by factors that can be as large as 6 or 7. The numerical results are tabulated in Table 2. It is also evident that the simulated AGB stars reach much brighter magnitudes than the observed ones. The excess of AGB stars is probably related to what has been already detected by Gullieuszik et al. (2008), Held et al. (2010), and Melbourne et al. (2010).

We have checked that these results depend little on the use of AGB stars by MATCH. Indeed, as shown in Table 2, the SFH derived when one hides the AGB stars in MATCH are very similar to those in which they are included and do not produce great changes in the predicted AGB/RGB ratios. Moreover, the comparison with models in which the metallicity is forced to not decrease with the galaxy age (the Z-inc option in MATCH) also produces similar results. We can only conclude that the problem resides in the AGB stellar models, and not in the observed samples or process of SFH recovery.

The observed galaxies always present, overall, a small fraction of intermediate-age stars (Table 2), or some moderately high metallicities, so that one might think that the results do not actually correspond to old metal-poor populations as it was intended to be. We know however that in dwarf galaxies the youngest (and more metal-rich) star formation is, as a rule, concentrated in the galaxy centers (e.g., Weisz et al. 2008; Stinson et al. 2009, and references therein; also K. M. Gilbert et al. 2011, in preparation). Therefore, for a subsample of our dwarf galaxies, we have selected the external rings for which the SFH is expected to be older than for the overall galaxy. The results are amended at the end of Table 2, for the no-AGB no-Z-inc option only. Although these outer regions are indeed slightly older than the entire galaxies, they show essentially identical $N_{\rm AGB}/N_{\rm RGB}$ ratios as the inner regions, suggesting that old populations dominate the CMDs at all radii. Therefore, the basic result for the excess of predicted AGB stars, by a factor of about 4, still remains in these data.

3.3. What is the Problem with Current TP-AGB Models?

The above-mentioned results were obtained with the use of MG07 TP-AGB evolutionary tracks, which constitute a quite non-standard grid of such models. They have considered, for the first time, features such as the changes in molecular opacities and mass-loss rates as the surface composition of TP-AGB stars passes from O- to C-rich, and the increase in the mass-loss rates as the long-period pulsation switches from the first overtone to the fundamental mode. Added to these improved prescriptions, there were attempts to calibrate the poorly known parameters of the models via the fitting of observational data. To be explicitly considered in the fitting were (1) the lifetimes of AGB stars as a function of stellar mass as derived from star counts in Magellanic Cloud clusters and (2) the C-star luminosity functions in both Clouds. After this calibration, other quantities were checked, as for instance the integrated colors of Magellanic Cloud clusters, and the initial–final mass relation derived from white dwarfs in the solar neighborhood. All these comparisons revealed an overall improvement in fits to data, even if there remained some problems, like for instance the integrated $V-K$ and $J-K$ colors being apparently too red as compared to the cluster data in the age interval from 10^8 to 4×10^8 yr (see the Appendix in Marigo et al. 2008).

One can separate the prescriptions used to build MG07 models into two broad groups: those which depend on the composition of stellar atmospheres—and especially on the C/O ratio—and those which do not. The first set of prescriptions is probably of secondary relevance for the present work, since we are dealing with stars in metal-poor and old stellar systems, most of which do not suffer convective dredge-up on the TP-AGB and hence are expected to be predominantly O-rich (of spectral types K and M). For the stars we are considering here, the TP-AGB lifetime and termination luminosity are crucially determined by the process of mass loss.

For O-rich stars, MG07 adopted a mass-loss prescription heavily based on Bowen & Willson (1991) dynamical model atmospheres for fundamental-mode pulsators, and with a dependence on metallicity as derived from Willson (2000). The initial period of TP-AGB mass loss as first-overtone pulsators was based on a set of relations derived from very few exploratory models by Bowen (1988). The procedure however was not straightforward, involving a large number of assumptions and fitting relations, caused by the different assumptions and ranges of parameters (e.g., the different underlying radius–luminosity–mass relation) between the original models from Bowen and Willson, and the synthetic TP-AGB models.

[14] http://www.stsci.edu/hst/acs/analysis/zeropoints

A detailed review of the literature, together with the results of Figure 2, suggests a complete revision of this scheme, as we now describe.

3.4. New TP-AGB Tracks

Our main problem is to reduce the lifetimes of TP-AGB tracks which, due to their low mass and metallicity, present relatively low luminosities and hot temperatures. Under such conditions, the classical dust-driven winds typically found in more luminous and cool AGB stars might be less efficient. In any case, we need to introduce some description for the "pre-dusty" winds (with rates $\dot{M}_{\rm pre\text{-}dust}$), i.e., before radiation pressure on dust grains becomes the main driving agent of mass loss (Elitzur & Ivezić 2001). Among the few such formulae which have been proposed in the literature, we decided to test the semi-empirical one by Schröder & Cuntz (2005)

$$\dot{M}_{\rm pre\text{-}dust} = \eta \frac{LR}{M} \left(\frac{T_{\rm eff}}{4000\,{\rm K}} \right)^{3.5} \left(1 + \frac{g_\odot}{4300\,g} \right) \ [M_\odot\,{\rm yr}^{-1}], \quad (1)$$

where R, M, and L are the stellar radius, mass, and luminosity expressed in solar units and g and $g_\odot$ indicate the stellar and solar surface gravity, respectively. This formula is a kind of Reimers (1975) law and was originally derived to describe the mass loss suffered by red giants under the assumption that the stellar wind originates from magneto-acoustic waves operating below the stellar chromosphere. The fitting parameter η is set to 0.8×10^{-13}, a value calibrated by Schröder & Cuntz (2005) to reproduce the morphology of horizontal branches in globular clusters.

The Schröder & Cuntz (2005) relation is employed from the beginning of the TP-AGB phase until a critical stage is met, i.e., the attainment of the minimum mass-loss rate, $\dot{M}^{\rm min}_{\rm dust}$, required for the development of a dust-driven wind. At each time step $\dot{M}^{\rm min}_{\rm dust}$ is evaluated numerically following the analysis by Gail & Sedlmayr (1987), from the condition

$$\alpha = \frac{L\,\kappa}{4\pi\,c G M} = 1\,, \quad (2)$$

which expresses the balance between the outward force caused by radiation pressure on dust and the inward gravitational pull of the star. Here c is the light speed, G is the gravitational constant, and κ is the flux-averaged mass extinction coefficient of the gas–dust mixture. Following Ferrarotti & Gail (2006), it is reasonable to assume that in the dust-driven outflow

$$\kappa = \kappa_{\rm gas} + \sum_i f_i \kappa_{{\rm dust},i}\,, \quad (3)$$

where the opacity contributions from the gas, $\kappa_{\rm gas}$, and dust species, $\kappa_{{\rm dust},i}$, are expressed as Rosseland means, while f_i represents the condensation degree of the ith dust species under consideration.

In our calculations, we consider different dust types depending on the star chemical type: silicates (pyroxene, olivine, and quartz) and iron in the case of M-stars (C/O $<$ 1), iron in the case of S-stars (C/O $\sim$1), and carbon, silicon carbide, and iron in the case of C-stars (C/O $>$ 1). The dust opacities are evaluated through the relations provided by Gail & Sedlmayr (1999) and Ferrarotti & Gail (2001, 2002), and the corresponding condensation degrees are estimated with the analytic fits proposed by Ferrarotti (2003).

These latter depend on the current $\dot{M}$, so that the minimum mass-loss rate of a dust-driven wind, $\dot{M}^{\rm min}_{\rm dust}$, is found iteratively through Equation (2).

As soon as $\dot{M}_{\rm pre\text{-}dust} \geqslant \dot{M}^{\rm min}_{\rm dust}$, the star enters the dust-driven wind regime, which is treated according to two formalisms:

1. Case A: based on Bowen & Willson (1991), but relaxing the metallicity dependence suggested by Willson (2000); and
2. Case B: based on Bedijn (1988), but with a somewhat different calibration of the parameters.

Case A for dust-driven winds is the same as in MG07, but for the correction factor describing the explicit metallicity dependence, which is left out in the new TP-AGB models. Nonetheless, an intrinsic metallicity effect still remains in the computed mass-loss rates, via the stellar surface parameters R and $T_{\rm eff}$. In fact at lower metallicities the atmospheres of AGB stars tend to be hotter and more compact. In practice, case A is meant to explore the hypothesis that the dust-driven winds may depend only mildly on the initial metal content.

Case B closely resembles the approach developed by Bedijn (1988), to which the reader is referred for all details. Briefly, assuming that the wind mechanism is the combined effect of two processes, i.e., radial pulsation and radiation pressure on the dust grains in the outermost atmospheric layers, Bedijn (1988) derived a formalism for the mass-loss rate as a function of basic stellar parameters, M, R, $T_{\rm eff}$, and the photospheric density $\rho_{\rm ph}$. Similarly to Bedijn (1988, see his Figure 1 and Appendix B) the free parameters have been calibrated on a sample of Galactic long-period variables with known mass-loss rate, pulsation period, stellar mass, radius, and effective temperature. More details about the fit procedure will be given elsewhere (P. Marigo et al. 2011, in preparation).

It should be noted that, in our calculations, R, $T_{\rm eff}$, and $\rho_{\rm ph}$ are derived from numerical integrations of complete envelope models extending from the photosphere down to the degenerate C–O core (see Marigo et al. 1999 for details). A key prerogative of our TP-AGB code is that at each time step, low-temperature opacities are computed, for the first time, on-the-fly with the ÆSOPUS tool (Marigo & Aringer 2009), thus assuring a full consistency with the surface chemical composition. In this way, we avoid the loss in accuracy that otherwise must be paid when interpolating on pre-computed opacity tables (the standard approach in stellar evolution models). This is important since low-temperature opacities are crucial in determining the position of a giant in the Hertszprung–Russell diagram. The opacities of carbon-rich stars (C/O $>$ 1), for instance, may be significantly higher, on average, than in oxygen-rich stars (C/O $<$ 1), so that the atmospheres of carbon-rich stars are usually less dense (and more extended) than those of oxygen-rich stars (Marigo 2002).

Figure 3 compares the MG07 results with the new ones, in terms of the (1) duration of the TP-AGB phase and (2) initial–final mass relation. It is evident that the significant reduction (by a typical factor of 3–4) of the TP-AGB lifetimes for initial masses $M_{\rm initial} \lesssim 0.9\,M_\odot$, as a consequence of the new prescriptions for the mass-loss rates. The shortening of the TP-AGB lifetimes derives from two concurring factors, i.e.: the non-negligible mass-loss rates already prior the onset of the dust-driven wind, and the higher efficiency during the dusty regime compared to MG07.

This fact is illustrated in Figure 4, showing the predicted evolution of the mass-loss rate for a model with initial mass $M_{\rm init} = 0.832\,M_\odot$ and metallicity $Z = 0.001$, according to the

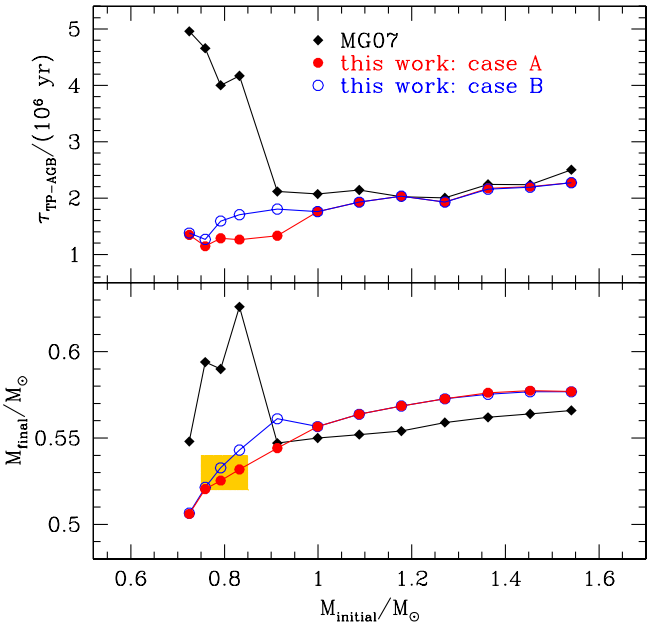

Figure 3. Comparison of AGB models with initial metallicity $Z = 0.001$ and for three different mass-loss prescriptions, as described in the text. Top panel: TP-AGB lifetimes as a function of the initial stellar mass. Bottom panel: final core masses left after the ejection of the envelope as a function of the initial stellar mass. The hatched rectangle shows the initial-final mass relation for the Galactic globular cluster M4, according to the recent white dwarf measurements by Kalirai et al. (2009).

(A color version of this figure is available in the online journal.)

three different choices of mass-loss formalisms discussed here. The evolutionary time is counted since the first thermal pulse up to the ejection of almost the entire envelope (calculations are stopped as soon as the envelope mass falls below 0.01 $M_\odot$). One critical feature common to cases A and B is that despite the low metallicity, the mass-loss rate $\dot{M}_{\rm pre\text{-}dust}$ predicted by the Schröder & Cuntz (2005) relation is already efficient, quickly increasing from $\approx 10^{-8}$ to $\approx 5 \times 10^{-7}\ M_\odot\ {\rm yr}^{-1}$ in a few thermal pulses. These rates are high enough to determine the ejection of the entire stellar mantle even before the development of the dust-driven wind (case B; bottom panel), or to favor its earlier onset (case A; middle panel). In general, the use of mass-loss prescription A leads to somewhat shorter TP-AGB lifetimes than case B.

Consequently, compared to MG07, the models with the new mass-loss descriptions predict a sizable reduction of the final masses, that are now mostly comprised in the interval $0.51 \lesssim (M_{\rm final}/M_\odot) \lesssim 0.55$ for $0.70 \lesssim (M_{\rm initial}/M_\odot) \lesssim 0.90$ (bottom panel of Figure 3). The most important result is that with no attempt to tune the mass loss, the new TP-AGB models are able to naturally recover the empirical initial–final mass relation of population II stars (bottom panel of Figure 3) as derived by Kalirai et al. (2009) from the first direct mass measurements of individual white dwarfs in the Galactic globular cluster M4. We have also verified that all metallicity sets in the range $0.0001 \leqslant Z \leqslant 0.001$ intersect the empirical data.

At larger initial masses, $0.9 \lesssim M_{\rm initial}/M_\odot \lesssim 1.5$, instead, there is a general agreement between the three sets of models, which are all predicted to make the transition to the C-rich domain (C/O $>$ 1), given the higher efficiency of the third dredge-up at the low metallicities here considered. In this case, the short TP-AGB lifetimes are controlled by the higher mass-loss rates for C-stars (following the reduction of $T_{\rm eff}$ as soon as C/O exceeds unity), while the flattening of the initial–final mass relation is mainly shaped by the deep dredge-up events. Interestingly, the three mass-loss prescriptions adopted here converge to similar results.

A general finding is that low-mass, low-metallicity models ($M_{\rm initial} \lesssim 1.0\ M_\odot$) would remain O-rich for all their TP-AGB evolution, experiencing non-negligible mass loss already before reaching the conditions to activate a dust-driven wind (not excluding that some passive dust could actually be present), so that the mass-loss mechanism on the TP-AGB should be ascribed to a different (unknown) driver, e.g., magneto-acoustic waves within the chromosphere (as discussed in Schröder & Cuntz 2005). In contrast, models with larger stellar masses, at roughly $M \geqslant 1.0\ M_\odot$, would quickly become C-rich as a consequence of the third dredge-up; under these conditions, the long-period pulsation and dust condensation would become efficient enough to trigger a radiative wind, with consequent strong enhancement of the mass loss and quick termination of the AGB phase. This prediction is in agreement with the results of detailed models of dust formation (Ferrarotti & Gail 2006).

Finally, we remark that we apply the above-described mass-loss formulae solely during the TP-AGB. We recognize that it would be important to explore the effect they also have for the RGB and early-AGB phases, but this is difficult in practice. It would require the calculation of more extended grids of evolutionary tracks, properly evaluating the mass loss during the evolution on the early-AGB, and including additional sets of horizontal branch models of smaller masses than presently available. This is very time consuming. Moreover, the evolutionary effects expected would be much smaller than those described above.

3.5. Results with the New TP-AGB Tracks

Figures 5 and 6 show the final result of using the new TP-AGB tracks in the simulation of ANGST galaxies, for cases A and B, respectively. It is evident that the reduction of TP-AGB lifetimes, and consequently of the TP-AGB termination luminosity, leads to a much better description of the data in both cases. For some galaxies such as ESO294-010, M81F6D1 and M81K64, the model-data agreement can be qualified as excellent, with simulated AGB numbers within the 67% confidence level of Poisson fluctuations in the data, and a good description of the luminosity function for AGB stars.

In a few other cases, however, the agreement is still not completely satisfactory, and the models tend to overestimate the AGB numbers by factors of up to 2, as for DDO113, DDO44, IKN, and DDO78. Note that in all these cases the observed AGB/RGB ratio is very small and close to its minimum value, which suggests that these galaxies are really dominated by very old populations. Therefore, we consider that the mismatch in the AGB/RGB ratios from the models might be attributable to the errors in the SFHs and metallicities of these galaxies, added of course to the residual mismatches in the stellar models of higher mass, and in the prescription for dust obscuration.

Finally, for the galaxies ESO0540-032, M81K61, SCL-DE1, DDO71, and M81F12D1, there is in general just a modest excess (smaller than ∼50%) in the predicted numbers of AGB stars. It is remarkable that this excess is generally more evident for the bright section of the AGB sequence, whereas close to the TRGB the numbers of predicted and observed AGB stars are in quite good agreement. We interpret the mismatch for bright AGB stars as being likely attributable to the younger population in these galaxies—with the causes being either in a slight overestimation of the lifetimes of the more massive TP-AGB models or in a

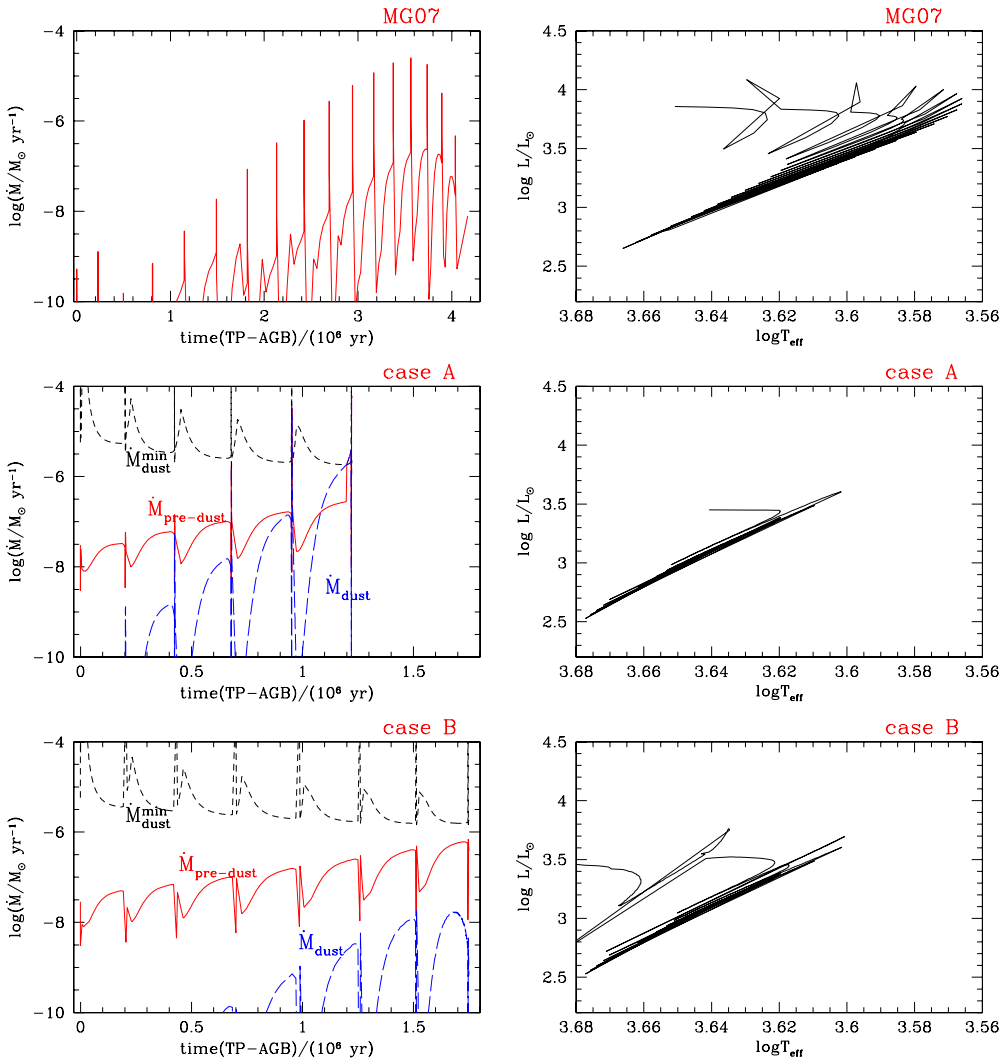

Figure 4. Evolution during the TP-AGB phase of a model with $M_{\rm init} = 0.832\,M_{\odot}$ (corresponding to a mass at the first thermal pulse $M_{\rm 1TP} = 0.80\,M_{\odot}$) and initial metallicity $Z = 0.001$, both in the mass-loss rate vs. time (left panels) and in the Hertzsprung–Russell diagram (right panels). The top panels show the results for the MG07 models, while the middle and bottom panels display the new calculations, for both formalisms of mass loss. The pulsation-dust-driven mass loss is represented with a dashed blue line, and $\dot{M}^{\rm min}_{\rm dust}$ is plotted with a dotted black line. As long as $\dot{M}_{\rm dust}$ keeps lower than $\dot{M}^{\rm min}_{\rm dust}$, the current mass-loss rate is given by $\dot{M}_{\rm pre\text{-}dust}$ following the Schröder & Cuntz (2005) formalism. Refer to the text for more explanation.

(A color version of this figure is available in the online journal.)

modest excess in the SFH derived from ANGST data for ages $\lesssim$3 Gyr.

From those galaxies in which there is good model–data agreement, we can conclude the following. They indicate that the TP-AGB lifetimes above the TRGB are of the order of 1.2–1.8 Myr (cf. Figure 3) for the low-mass, low-metallicity AGB stars ($M \lesssim 1\ M_{\odot}$, [Fe/H] $\lesssim -1.2$) which are typically being sampled. The need for such a reduction in TP-AGB lifetimes, with respect to those in the MG07 models, has already been indicated by Gullieuszik et al. (2008) in their study of the old metal-poor Leo II dSph, and to a lesser extent also by Held et al. (2010) and Melbourne et al. (2010) while studying metal-poor galaxies with somewhat younger SFHs. On the other hand, it is quite reassuring that the final core masses of our best-fitting AGB models are between 0.51 and 0.55 $M_{\odot}$ (again for low-mass stars, with say $M \lesssim 1\ M_{\odot}$), which is in good agreement with the observed masses of white dwarfs in globular clusters of the MW (of $0.53 \pm 0.01\ M_{\odot}$; cf. Kalirai et al. 2009). This latter indication also agrees with the low initial–final mass relation derived from the number counts of hot white dwarfs—mostly from the thin disk—in GALEX wide area surveys (Bianchi et al. 2010). Thus, we find that the dramatic reduction in the lifetimes and final masses of our TP-AGB models are well in line with the indications from independent data.

Whereas we have tested two different prescriptions for the mass-loss rate at the dust-driven phase, both turn out to provide essentially the same results, with case A reproducing our data for old metal-poor galaxies just slightly better than case B. However, the differences between these two prescriptions are expected to increase for stars of masses $\gtrsim 2\ M_{\odot}$, which reach significantly higher luminosities. Therefore, they need to be tested in galaxies containing young populations, which will be the subject of forthcoming papers.

4. CLOSING REMARKS

In this work, we have derived strong constraints on the lifetimes of low-mass, metal-poor AGB stars via the study of their numbers and luminosity functions in galaxy regions with a predominantly old and metal-poor SFH. The AGB lifetimes at

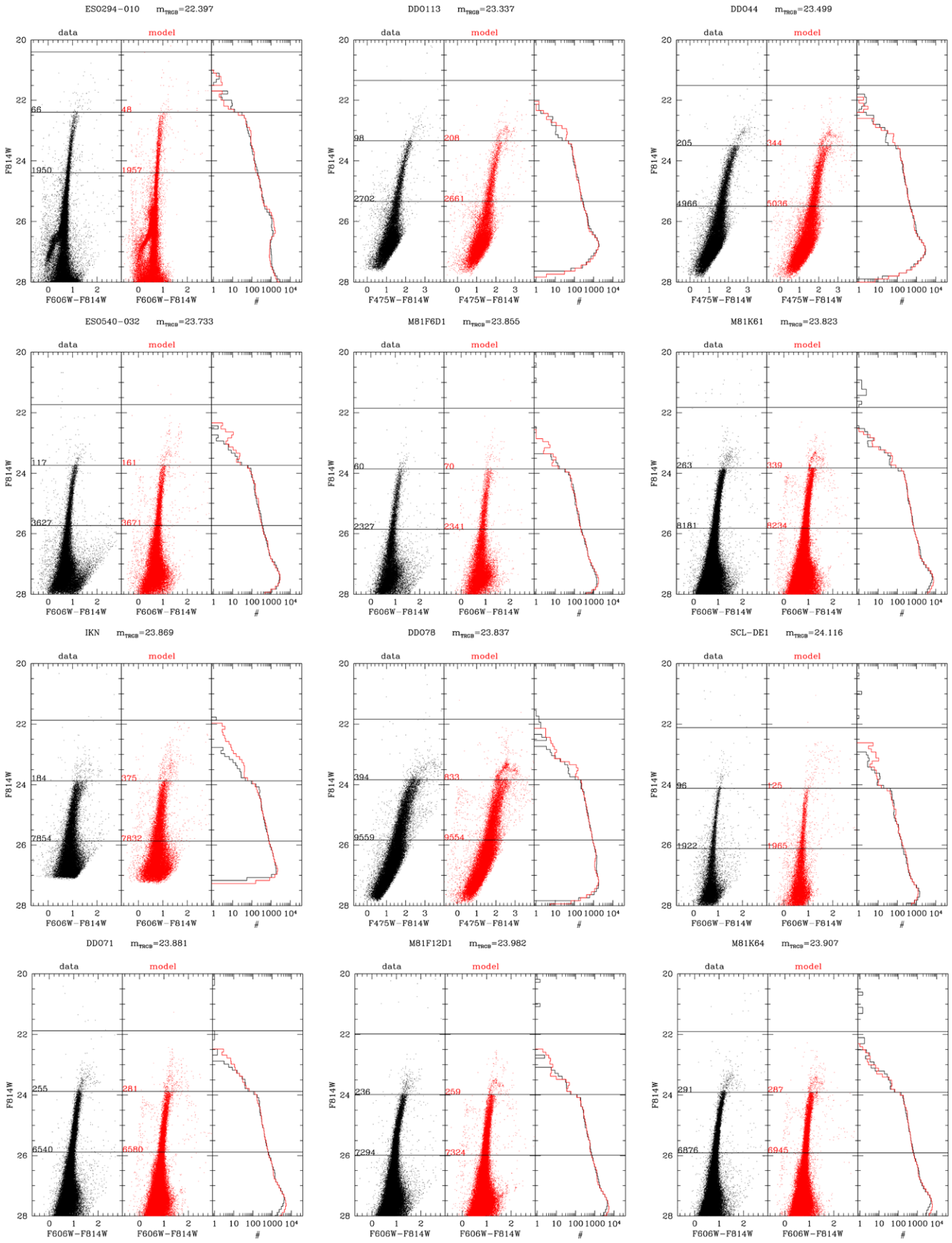

Figure 5. Same as Figure 2, but now using our best TP-AGB models, for case A mass loss.
(A color version of this figure is available in the online journal.)

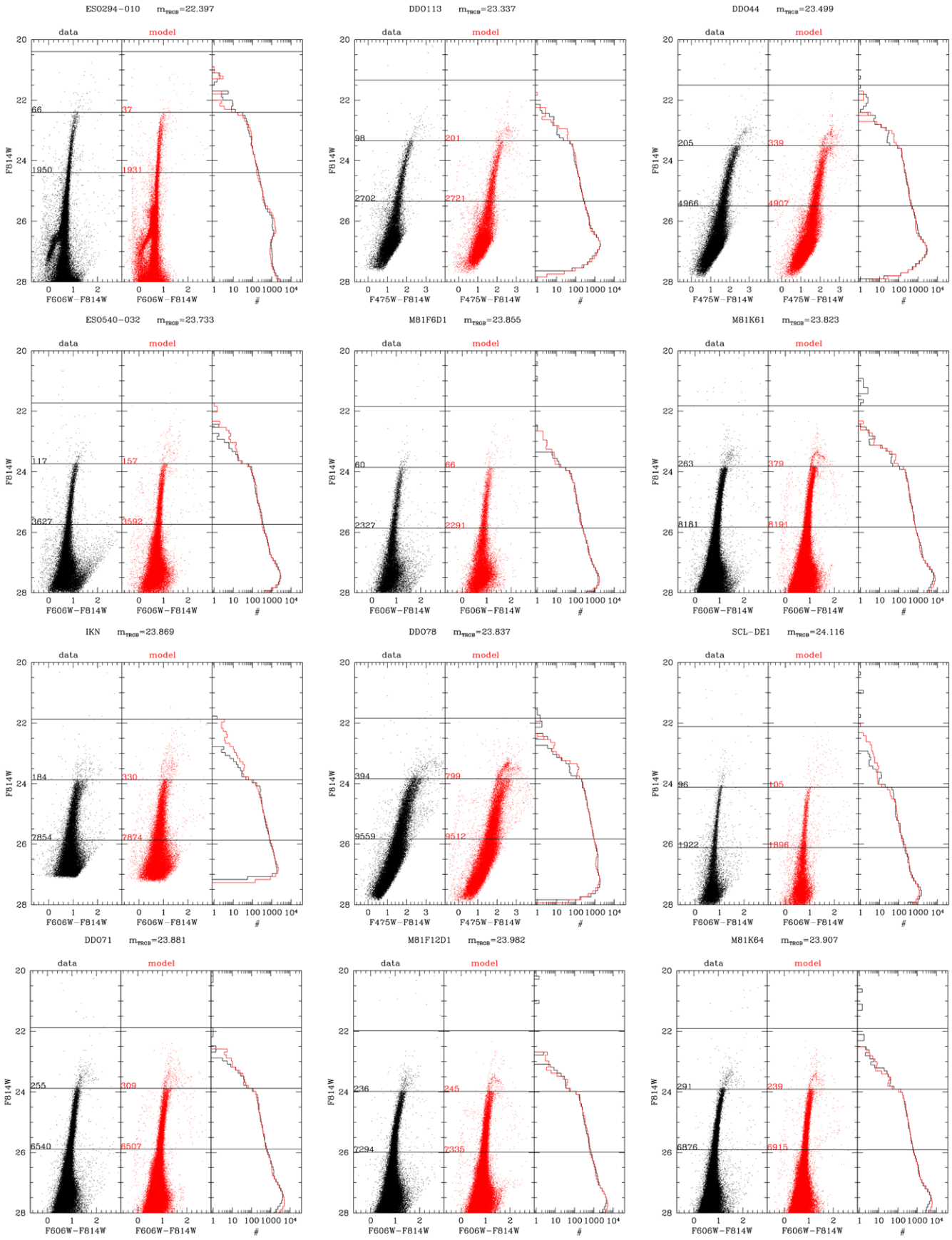

Figure 6. Same as Figure 2, but now using the TP-AGB models for case B mass loss.
(A color version of this figure is available in the online journal.)

magnitudes brighter than the TRGB turn out to be between 1.2 and 1.8 Myr for stellar masses of $M \lesssim 1\ M_{\odot}$, at metallicities [Fe/H] $\lesssim -1.2$. Indeed, TP-AGB evolutionary tracks with these lifetimes are able to reproduce quite well the low AGB/RGB number ratios in a subsample of these galaxies, as well as their luminosity functions. In some other cases, the agreement is still not perfect, but the new models perform significantly better than the previous MG07 ones. Although we have tested just two possible alternative prescriptions for mass loss, they both produce a quite similar reduction in the AGB lifetimes, as well as similar final masses for the resulting white dwarfs.

Whereas the constraints we derive may apply to quite a limited range of stellar masses and metallicities, they also represent an important step toward a robust calibration of the lifetimes of TP-AGB stars at all masses and metallicities. Indeed, with this single point in mass–metallicity space we can discard some of the already proposed formulae for the mass loss on the AGB, for instance the Bowen & Willson (1991) and Willson (2000) ones as implemented in MG07. Moreover, we can use this result as a reference point to start a more thorough calibration of the AGB lifetimes at regimes of increasing masses and metallicities, making use of additional galaxies with the presence of younger SFH and more metal-rich giant branches. Such an extension of the AGB calibration, however, cannot proceed via the analysis of optical data only, as performed in this paper. It requires *at least* the use of near-infrared photometry in order to sample the most massive and evolved AGB stars, as well as those of higher metallicities. Indeed, we are presently collecting near-infrared data with the new *HST*/WFC3 camera (IR channel), for some dozens of ANGST galaxies with a well-measured SFH. Forthcoming papers will discuss the problem of improving AGB models in the light of these new data.

The present TP-AGB tracks surely represent an improvement in our sets of isochrones and tools to simulate stellar populations. For this reason they are being included as an alternative to the MG07 models, in the CMD[15] and TRILEGAL[16] Web interfaces, which provide isochrones and simulated photometry of resolved stellar populations in a wide variety of filter systems.

L.G. and P.M. acknowledge financial support from contract ASI-INAF I/016/07/0 and INAF/PRIN07 CRA 1.06.10.03. B.F.W., J.J.D., P.R., and D.R.W. acknowledge financial support from HST GO-10915. K.M.G. acknowledges support from HST GO-10945. P.R. acknowledges the Achievement Rewards for College Scientists (ARCS) Fellowship. J.J.D. and P.R. were partially supported by AR-10945, GO-11718, and GO-11307.

This work is based on observations made with the NASA/ESA *Hubble Space Telescope*, obtained from the data archive at the Space Telescope Science Institute. Support for this work was provided by NASA through grant Nos. GO-10915 and GO-10945 from the Space Telescope Science Institute, which is operated by AURA, Inc., under NASA contract NAS 5-26555. This research has made use of the NASA/IPAC Infrared Science Archive and the NASA/IPAC Extragalactic Database (NED), which are both operated by the Jet Propulsion Laboratory, California Institute of Technology, under contract with the National Aeronautics and Space Administration. This research has made extensive use of NASA's Astrophysics Data System Bibliographic Services.

Facilities: HST (ACS, WFPC2)

[15] http://stev.oapd.inaf.it/cmd
[16] http://stev.oapd.inaf.it/trilegal

REFERENCES

Aringer, B., Girardi, L., Nowotny, W., Marigo, P., & Lederer, M. T. 2009, A&A, 503, 913
Bedijn, P. J. 1988, A&A, 205, 105
Bianchi, L., et al. 2010, MNRAS, submitted
Blum, R. D., et al. 2006, AJ, 132, 2034
Bohlin, R. C. 2007, Photometric Calibration of the ACS CCD Cameras, Science Report ACS 2007-06 (Baltimore, MD: STScI), http://www.stsci.edu/hst/acs/documents/isrs/isr0706.pdf
Bolatto, A. D., et al. 2007, ApJ, 655, 212
Bowen, G. H. 1988, ApJ, 329, 299
Bowen, G. H., & Willson, L. A. 1991, ApJ, 375, L53
Boyer, M. L., Skillman, E. D., van Loon, J. T., Gehrz, R. D., & Woodward, C. E. 2009a, ApJ, 697, 1993
Boyer, M. L., et al. 2009b, ApJ, 705, 746
Boyer, M. L., et al. 2010, ApJ, 711, L99
Castelli, F., & Kurucz, R. L. 2003, in IAU Symp. 210, Modelling of Stellar Atmospheres, ed. N. Piskunov, W. W. Weiss, & D. F. Gray (Cambridge: Cambridge Univ. Press), 20
Cioni, M., & Habing, H. J. 2003, A&A, 402, 133
Cioni, M., et al. 2000, A&AS, 144, 235
Conroy, C., & Gunn, J. E. 2010, ApJ, 712, 833
Conroy, C., Gunn, J. E., & White, M. 2009, ApJ, 699, 486
Cordier, D., Pietrinferni, A., Cassisi, S., & Salaris, M. 2007, AJ, 133, 468
Dalcanton, J. J., et al. 2009, ApJS, 183, 67
Dolphin, A. E. 2000, PASP, 112, 1383
Dolphin, A. E. 2002, MNRAS, 332, 91
Elitzur, M., & Ivezić, Ž. 2001, MNRAS, 327, 403
Eminian, C., Kauffmann, G., Charlot, S., Wild, V., Bruzual, G., Rettura, A., & Loveday, J. 2008, MNRAS, 384, 930
Ferrarotti, A. S. 2003, PhD thesis, Naturwissenschaftlich-Mathematische Gesamtfakultät der Universität Heidelberg
Ferrarotti, A. S., & Gail, H. 2001, A&A, 371, 133
Ferrarotti, A. S., & Gail, H. 2002, A&A, 382, 256
Ferrarotti, A. S., & Gail, H. 2006, A&A, 447, 553
Fluks, M. A., Plez, B., Thé, P. S., de Winter, D., Westerlund, B. E., & Steenman, H. C. 1994, A&AS, 105, 311
Frogel, J. A., & Elias, J. H. 1988, ApJ, 324, 823
Frogel, J. A., Mould, J., & Blanco, V. M. 1990, ApJ, 352, 96
Frogel, J. A., & Whitelock, P. A. 1998, AJ, 116, 754
Gail, H., & Sedlmayr, E. 1987, A&A, 177, 186
Gail, H., & Sedlmayr, E. 1999, A&A, 347, 594
Gallart, C., Zoccali, M., & Aparicio, A. 2005, ARA&A, 43, 387
Girardi, L., Bertelli, G., Bressan, A., Chiosi, C., Groenewegen, M. A. T., Marigo, P., Salasnich, B., & Weiss, A. 2002, A&A, 391, 195
Girardi, L., Groenewegen, M. A. T., Hatziminaoglou, E., & da Costa, L. 2005, A&A, 436, 895
Girardi, L., & Marigo, P. 2007a, A&A, 462, 237
Girardi, L., & Marigo, P. 2007b, in ASP Conf. Ser. 378, Why Galaxies Care About AGB Stars: Their Importance as Actors and Probes, ed. F. Kerschbaum, C. Charbonnel, & R. F. Wing (San Francisco, CA: ASP), 20
Girardi, L., et al. 2008, PASP, 120, 583
Groenewegen, M. A. T. 2006, A&A, 448, 181
Groenewegen, M. A. T., Sloan, G. C., Soszyński, I., & Petersen, E. A. 2009, A&A, 506, 1277
Gullieuszik, M., Held, E. V., Rizzi, L., Girardi, L., Marigo, P., & Momany, Y. 2008, MNRAS, 388, 1185
Held, E. V., Gullieuszik, M., Rizzi, L., Girardi, L., Marigo, P., & Saviane, I. 2010, MNRAS, 404, 1475
Jackson, D. C., Skillman, E. D., Gehrz, R. D., Polomski, E., & Woodward, C. E. 2007a, ApJ, 656, 818
Jackson, D. C., Skillman, E. D., Gehrz, R. D., Polomski, E., & Woodward, C. E. 2007b, ApJ, 667, 891
Kalirai, J. S., Saul Davis, D., Richer, H. B., Bergeron, P., Catelan, M., Hansen, B. M. S., & Rich, R. M. 2009, ApJ, 705, 408
Kamath, D., Wood, P. R., Soszyński, I., & Lebzelter, T. 2010, MNRAS, 1190
Lagadec, E., Zijlstra, A. A., Matsuura, M., Menzies, J. W., van Loon, J. T., & Whitelock, P. A. 2008, MNRAS, 383, 399
Lebzelter, T., Lederer, M. T., Cristallo, S., Hinkle, K. H., Straniero, O., & Aringer, B. 2008, A&A, 486, 511
Lebzelter, T., Posch, T., Hinkle, K., Wood, P. R., & Bouwman, J. 2006, ApJ, 653, L145
Lebzelter, T., & Wood, P. R. 2007, A&A, 475, 643
Mack, J., Gilliland, R. L., Anderson, J., & Sirianni, M. 2007, WFC Zero-points at −80°C, Science Report ACS 2007-02 (Baltimore, MD: STScI), http://www.stsci.edu/hst/acs/documents/isrs/isr0702.pdf

Maraston, C. 2005, MNRAS, 362, 799
Maraston, C., Daddi, E., Renzini, A., Cimatti, A., Dickinson, M., Papovich, C., Pasquali, A., & Pirzkal, N. 2006, ApJ, 652, 85
Marigo, P. 2002, A&A, 387, 507
Marigo, P., & Aringer, B. 2009, A&A, 508, 1539
Marigo, P., & Girardi, L. 2007, A&A, 469, 239
Marigo, P., Girardi, L., & Bressan, A. 1999, A&A, 344, 123
Marigo, P., Girardi, L., Bressan, A., Groenewegen, M. A. T., Silva, L., & Granato, G. L. 2008, A&A, 482, 883
McDonald, I., van Loon, J. T., Decin, L., Boyer, M. L., Dupree, A. K., Evans, A., Gehrz, R. D., & Woodward, C. E. 2009, MNRAS, 394, 831
McDonald, I., van Loon, J. T., Dupree, A. K., & Boyer, M. L. 2010, MNRAS, 405, 1711
Melbourne, J., Williams, B., Dalcanton, J., Ammons, S. M., Max, C., Koo, D. C., Girardi, L., & Dolphin, A. 2010, ApJ, 712, 469
Méndez, B., Davis, M., Moustakas, J., Newman, J., Madore, B. F., & Freedman, W. L. 2002, AJ, 124, 213
Nikolaev, S., & Weinberg, M. D. 2000, ApJ, 542, 804
Pessev, P. M., Goudfrooij, P., Puzia, T. H., & Chandar, R. 2008, MNRAS, 385, 1535
Raimondo, G. 2009, ApJ, 700, 1247
Reimers, D. 1975, Mem. Soc. R. Sci. Liège, 8, 369
Salpeter, E. E. 1955, ApJ, 121, 161
Schlegel, D. J., Finkbeiner, D. P., & Davis, M. 1998, ApJ, 500, 525
Schröder, K., & Cuntz, M. 2005, ApJ, 630, L73
Stinson, G. S., Dalcanton, J. J., Quinn, T., Gogarten, S. M., Kaufmann, T., & Wadsley, J. 2009, MNRAS, 395, 1455
van Loon, J. T., Marshall, J. R., & Zijlstra, A. A. 2005, A&A, 442, 597
van Loon, J. T., McDonald, I., Oliveira, J. M., Evans, A., Boyer, M. L., Gehrz, R. D., Polomski, E., & Woodward, C. E. 2006, A&A, 450, 339
Weinberg, M. D., & Nikolaev, S. 2001, ApJ, 548, 712
Weisz, D. R., Skillman, E. D., Cannon, J. M., Dolphin, A. E., Kennicutt, R. C., Jr., Lee, J., & Walter, F. 2008, ApJ, 689, 160
Williams, B. F., et al. 2009, AJ, 137, 419
Willson, L. A. 2000, ARA&A, 38, 573